Using Machine Learning for formulating new wall functions for Large Eddy Simulation: A First Attempt

L. Davidson
Div. of Fluid Dynamics
Mechanics and Maritime Sciences (M2)
Chalmers University of Technology, Gothenburg, Sweden

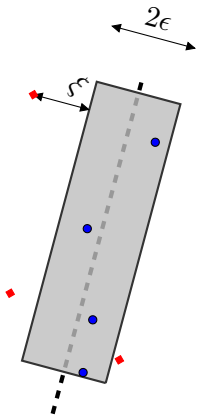

Sketch of support vector regression (SVR). Data point inside (•) and outside (■) the tube (gray area). The gray dashed line is the hyperplane (regression plane) predicted by `svrLINEAR`.

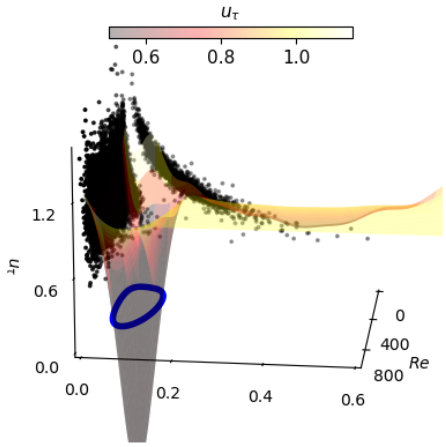

Colored surface is the hyperplane. I get non-physical (negative) friction velocities, u_τ, predicted by `svrLINEAR` because I use too small "slack" (i.e. too large C). Thick blue line: $u_\tau = 0$.

Abstract

Machine learning is used for developing wall functions for Large Eddy Simulations (LES). I use Direct Numerical Simulation (DNS) of fully-developed channel flow at frictional Reynolds number of 800 to create a database. This database is using as a training set for the machine learning method (support vector regression). The input data (i.e. the influence parameters) are the local Reynolds number, the non-dimensional velocity gradient and the time-averaged y^+ value. The machine learning method is trained to predict the wall shear stress.

The support vector regression methods in Python are used. The trained machine learning model is saved to disk and it is subsequently uploaded into the Python CFD code **pyCALC-LES** (Davidson, 2021). LES is carried out on coarse – and semi-course – near-wall meshes and the wall-shear stress is predicted using the developed machine learning models.

Contents

1 Introduction **4**

2 Direct Numerical Simulations (DNS) **5**

3 Large Eddy Simulation (LES) **7**

4 Standard wall functions **8**

5 The machine learning methods **9**
5.1 Python code 12

6 Results **14**
6.1 $Re_\tau = 2\,000$ 14
6.2 $Re_\tau = 5\,200$ 17
6.3 $Re_\tau = 5\,200$ with a stretching of 1.08. 19
6.4 $Re_\tau = 5\,200$ with a stretching of 1.11. 19

7 Conclusions **22**

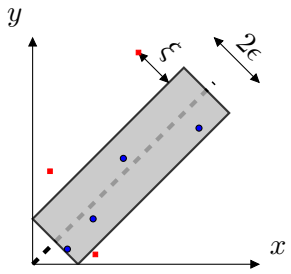

Figure 1: Sketch of support vector regression. Data point inside (●) and outside (■) the tube (gray area). The gray dashed line is the predicted solution which is called the hyperplane which may be linear (`svrLINEAR`) or non-linear (`svr`).

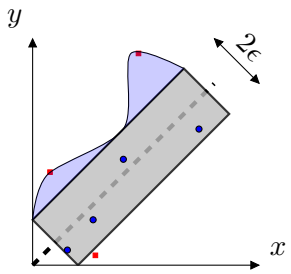

Figure 2: Sketch of vector regression. A large C enlarges the area of the tube (blue area).

1 Introduction

Machine learning is a method where known data are used for teaching the algorithm to classify a set of data. The data may be photographs where the machine learning algorithm should recognize, for example, traffic lights or traffic signs (Rao and Desai, 2021). Another example may be ECG signals where the machine learning algorithm should recognize certain unhealthy conditions of the heart (Lindholm et al., 2022). A third example is detecting fraud for credit card payments (Rachana et al., 2021). Machine learning methods such as Support Vector Machines (SVM) and neural networks are often used for solving this type of problems.

The examples above are classification problems using supervised learning (i.e. learning to recognise a traffic light, an unhealthy heart, learn what a customers usual credit card payment looks like). However, in the present work input and output are numerical values. In this case, machine learning in the form of regression methods should be used (Lindholm et al., 2022); I will use support vector regression (SVR) methods available in Python.

In SVR a regression mult-dimensional "surface" is created which has as many dimensions as number of influence parameters (in the present work I use one, two

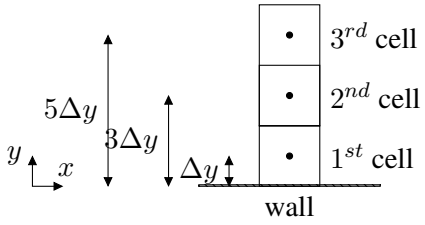

Figure 3: DNS database.

or three influence parameters). Let's make a simple example. In Fig. 1 there is one influence parameter, x, and one parameter to predict, y. Two main input parameters may be given to the SVR methods. The first is ϵ which determines the width of the tube around the hyperplane [1]. Points that lie inside this tube are considered as correct predictions and are not penalized by the algorithm. The support vectors are the points that lie outside the tube The second parameter given to SVR models is the C value. It controls the "slack" (ξ), see Fig. 1, which is the distance to points outside the tube. If C is increased the size of the tube is increased so that some or all of the data points are located inside the tube. It will be shown in Section 5 that the parameter C may have a large influence on the form of the hyperplane.

There are not many studies in the literature on machine-learning for improving wall functions. In (Tieghi et al., 2020) they use a time-averaged high-fidelity LES simulation which is used to train a neural network for improving the predicted modeled turbulent kinetic used in wall functions in RANS. Ling et al. (2017) use neural network to improve the predicted wall pressure to be used in fluid-structure interactions. They target it the wall pressure spectrum and the input parameters are the pressure power spectra above the wall. In (Dominique et al., 2022) they use neural network to predict the wall pressure spectra. Their input data include are boundary-layer thicknesses (physical, displacement and momentum), streamwise pressure gradient and wall shear stress which are taken from experiments and high-fidelity DNS/LES in the literature.

2 Direct Numerical Simulations (DNS)

To create a database which can be used for training the SVR I will carry out a DNS of fully-developed channel flow. The Navier-Stokes equations read

$$\frac{\partial v_i}{\partial x_i} = 0 \tag{1}$$

$$\frac{\partial v_i}{\partial t} + \frac{\partial}{\partial x_j}(v_i v_j) = -\frac{\partial p}{\partial x_i} + \nu \frac{\partial^2 v_i}{\partial x_j \partial x_j} \tag{2}$$

[1] A hyperplane is a plane whose number of dimension is the same the number of influence parameters. For example, a two-dimensional hyperplane has two influence parameters.

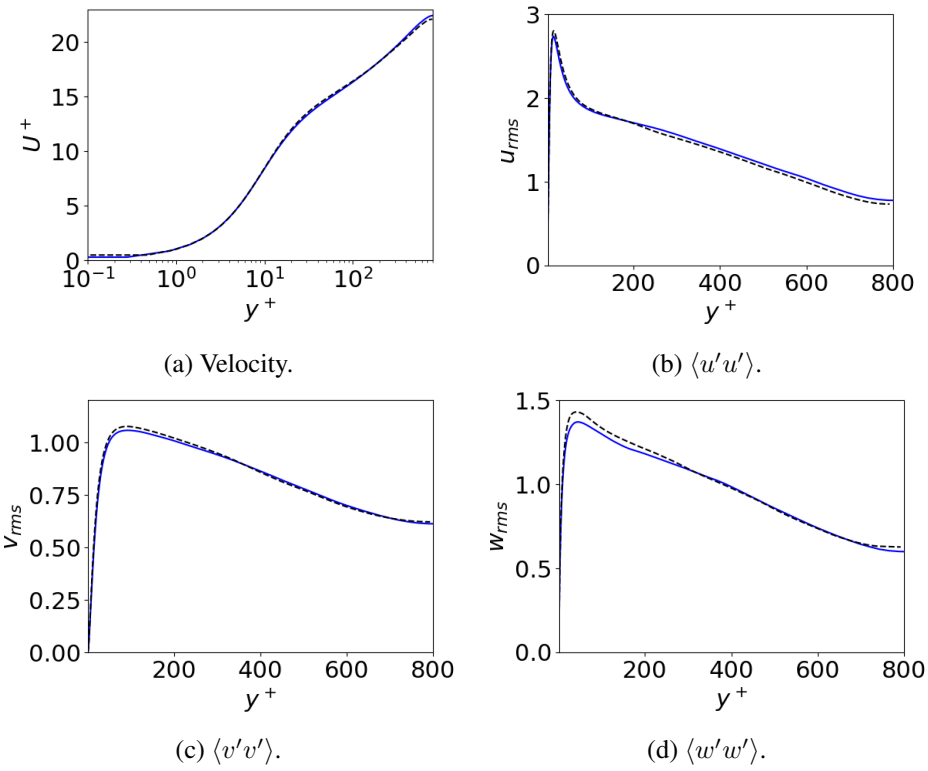

(a) Velocity.

(b) $\langle u'u' \rangle$.

(c) $\langle v'v' \rangle$.

(d) $\langle w'w' \rangle$.

Figure 4: Channel flow at $Re_\tau = 800$. —— : Present DNS; - - - : DNS data (Tanahashi et al., 2004).

	$\langle \Delta y^+ \rangle$
Location 1	5
Location 2	13
Location 3	24
Location 4	39
Location 5	58
Location 6	85

Table 1: DNS database for high y^+ wall functions. Δy is defined in Fig. 3. The locations of the second and the third cell is obtained from Fig. 3.

An incompressible, finite volume code is used (Davidson and Peng, 2003; Davidson, 2018) to solve Eqs. 1 and 2. The convective terms in the momentum equations are discretized using central differencing. The Crank-Nicolson scheme is used for time discretization of all equations. The numerical procedure is based on an implicit, fractional step technique with a multigrid pressure Poisson solver (Emvin, 1997) and a non-staggered grid arrangement.

The size of the channel is $x_{max} = 2\pi$ (streamwise, x or x_1), $y_{max} = 2$ (wall normal, y or x_2) and $z_{max} = 1.6$ (spanwise, z or x_3). The mesh has $386 \times 258 \times 386$ and the Reynolds number is 800 based on the friction velocity, $\langle u_\tau \rangle$ ($\langle \cdot \rangle$ denotes average in time, x_1 and x_3), and the half-channel width, δ.

Figure 4 presents comparison of the predicted velocity field and RSM fluctuations with DNS by Tanahashi et al. (2004) and – as can be seen – the agreement is very good.

When creating the instantaneous velocity, $\bar{U}$,, for the database, I integrate over a distance in y direction (see Fig. 3). The streamwise velocities for the 1^{st}, 2^{nd} and 3^{rd} cells are computed as

$$\bar{U}_{1^{st}} = \frac{1}{2\Delta y}\int_0^{2\Delta y} u dy, \quad \bar{U}_{2^{nd}} = \frac{1}{2\Delta y}\int_{2\Delta y}^{4\Delta y} u dy, \quad \bar{U}_{3^{rd}} = \frac{1}{2\Delta y}\int_{4\Delta y}^{6\Delta y} u dy \quad (3)$$

where Δy is representative of a typical cell size in a LES simulation using wall functions. The six locations of the first cell are given in Table 1. The locations of the second and third cells are shown in Fig. 3.

3 Large Eddy Simulation (LES)

The LES equations read

$$\begin{aligned} \frac{\partial \bar{v}_i}{\partial x_i} &= 0 \\ \frac{\partial \bar{v}_i}{\partial t} + \frac{\partial}{\partial x_j}\left(\bar{v}_i \bar{v}_j\right) &= -\frac{\partial \bar{p}}{\partial x_i} + \frac{\partial}{\partial x_j}\left[(\nu + \nu_{sgs})\frac{\partial \bar{v}_i}{\partial x_j}\right] \end{aligned}$$

	$\langle \Delta y^+ \rangle$
Location 1	3
Location 2	9
Location 3	16
Location 4	25
Location 5	37
Location 6	52

Table 2: DNS database for low y^+ wall functions. Δy is defined in Fig. 3. The locations of the second and the third cell is obtained from Fig. 3.

where the Smagorinsky model is used

$$\begin{aligned} \nu_{sgs} &= (C_S\Delta)^2 \sqrt{2\bar{s}_{ij}\bar{s}_{ij}} \equiv (C_S\Delta)^2 |\bar{s}| \\ \bar{s}_{ij} &= \frac{1}{2}\left(\frac{\partial \bar{v}_i}{\partial x_j} + \frac{\partial \bar{v}_j}{\partial x_i}\right) \end{aligned}$$

with $C_S = 0.1$. The SGS viscosity near the wall is dampened by using the RANS length scale as an upper limit, i.e.

$$\Delta = \min\left\{(\Delta V_{IJK})^{1/3}, \kappa n\right\}$$

where n is the distance to the nearest wall.

The finite volume code **pyCALC-LES** (Davidson, 2021) is used. It is written in Python and is fully vectorized (i.e. no `for` loops). The solution procedure is based on fractional step. Second-order central differencing is used in space and the Crank-Nicolson scheme in time. All discretized equation are solved on the GPU using the Algebraic MultiGrid (AMG) solver `pyAMGx` (Olson and Schroder, 2018). The reason why **pyCALC-LES** is not used for the DNS simulations in Section 2 is that the memory of the GPU on the author's desktop is too small.

4 Standard wall functions

The machine-learning wall functions will be compared to the standard wall functions which are based on log-law, i.e.

$$\frac{\bar{v}_1}{u_\tau} = \frac{1}{\kappa}\ln\left(\frac{Eu_\tau\Delta y}{\nu}\right) \equiv \frac{1}{\kappa}\ln\left(Ey^+\right), \quad E = 9.0 \tag{4}$$

where Δy is given by Fig. 3 and subscript P denotes wall-adjacent cell. I compute the friction velocity from Equation 4 as

$$u_\tau = \frac{\kappa \bar{v}_{1,P}}{\ln(Eu_\tau\Delta y/\nu)} \tag{5}$$

which is solved by iterating a couple of times. If $y^+ < 11.63$, the linear law is used

$$u_\tau = \left(\nu \frac{\partial \bar{v}_1}{\partial x_2}\bigg|_{y=0} \right)^{1/2} \tag{6}$$

5 The machine learning methods

As indicated in the introduction, I will use SVR (Support Vector Regression). Two different packages are used, `svr` and `svrLINEAR`, both available in Python. The former method is non-linear and the latter is linear. The machine learning method consists of a learning part and a testing part. In the learning part, the machine learning method is trained and in the testing part it is tested.

First, I need to determine which input variable (influence parameters) that should be used. In standard wall functions, the input parameters are wall-parallel velocity, $\bar{v}_{1,P}$ and the non-dimensional wall distance, y^+ (which includes the friction velocity, u_τ); the output is the friction velocity. Hence, the friction is both input and output. In a machine learning method, it is probably not a good idea to let a parameter be included in both an input and output parameter. In order to make the machine learning method as general as possible, the input variables should be non-dimensional. The following influence (i.e. input) parameters are evaluated:

- the local Reynolds number, $\dfrac{\bar{U}_{1^{st}} \Delta y}{\nu}$
- the velocity gradient, $\dfrac{\partial \bar{U}}{\partial y} = \dfrac{\bar{U}_{2^{nd}} - \bar{U}_{1^{st}}}{2\Delta y}$; it is made non-dimensional by ν and $\bar{U}_{1^{st}}$ as
$$\left(\frac{\partial \bar{U}}{\partial y} \right)_{non} = \frac{\partial \bar{U}}{\partial y} \frac{\nu}{\bar{U}^2_{1^{st}}} \tag{7}$$
- the averaged non-dimensional wall distance, $\dfrac{\langle u_\tau \rangle \Delta y}{\nu}$

where $\bar{U}_{1^{st}}$ and $\bar{U}_{2^{nd}}$ are computed from Eq. 3. It may be noted that the velocity at the third point, see Fig. 3, is not used when computing these three input parameters.

Next, I will train the machine learning method using the DNS data created in Section 2. I start with `svrLINEAR`. 100 000 independent samples of $\bar{U}_{1^{st}}$ and $\bar{U}_{2^{nd}}$ are used at each of the six locations, see Table 1 and Fig. 3 together with the output parameter, u_τ. I have also evaluated to use 10 000 samples and I get identical results. I could probably use even fewer samples. I pick 80% of the data randomly and define that as the training set. The remaining 20% is then used for testing, i.e. predicting.

Figure 5 shows predicted friction friction velocities and the hyperplanes for `svrLINEAR` using the velocity gradient and local Reynolds number as influence (i.e. input) parameters for different C and ϵ (these two parameters determines the

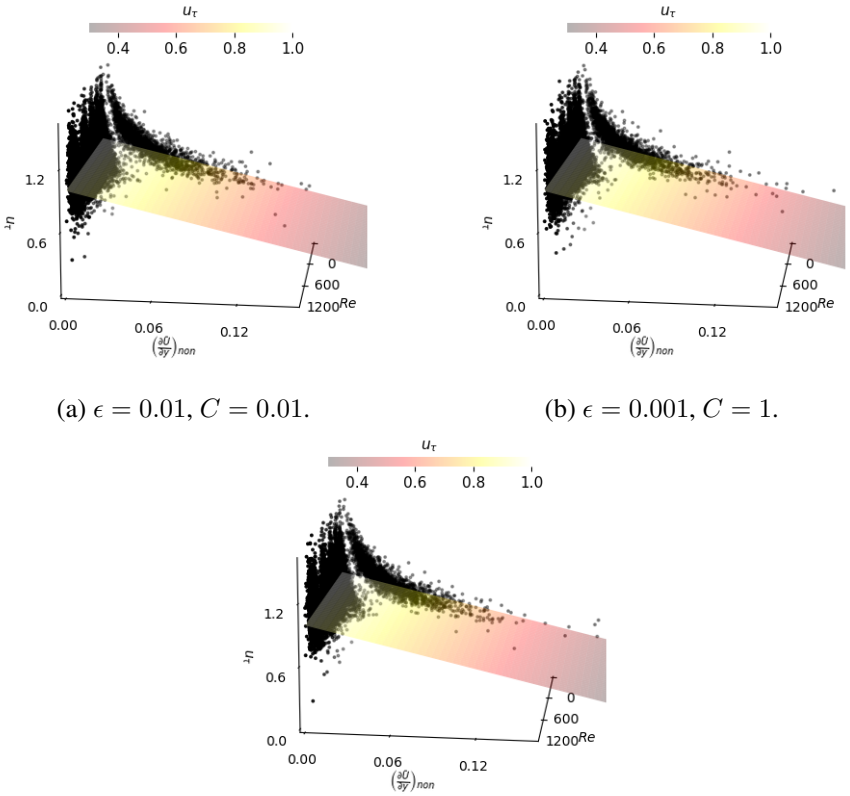

(a) $\epsilon = 0.01$, $C = 0.01$.

(b) $\epsilon = 0.001$, $C = 1$.

(c) $\epsilon = 0.001$, $C = 0.01$.

Figure 5: Predicted friction velocity with `svrLINEAR` using high y^+ data. ▪ : predicted friction velocity; 3D surface: hyperplane colored with u_τ

.

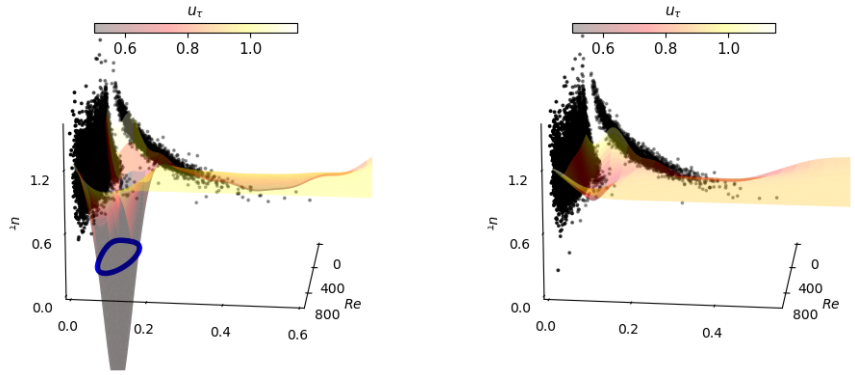

(a) $\epsilon = 0.1$, $C = 0.1$. Thick blue line: $u_\tau = 0$.

(b) $\epsilon = 0.1$, $C = 0.01$.

Figure 6: Predicted friction velocity with `svr` using low y^+ data, see Table 1. 3D view. ▪ : Predicted friction velocity; 3D surface: hyperplane colored with u_τ

.

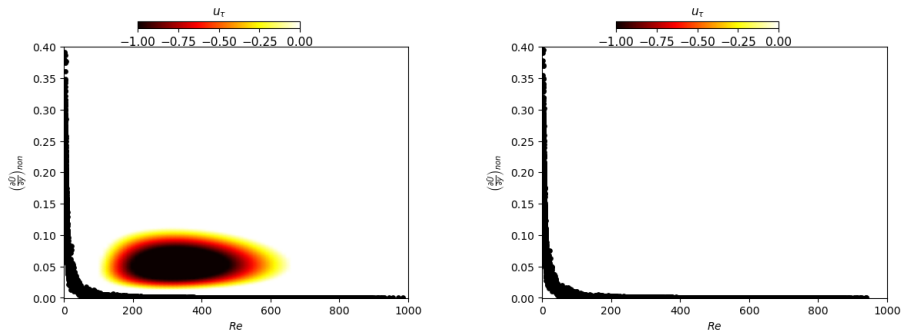

(a) $\epsilon = 0.1$, $C = 0.1$.

(b) $\epsilon = 0.1$, $C = 0.01$.

Figure 7: Predicted friction velocity with `svr` using low y^+ data, see Table 2. 2D view. ▪ : Predicted friction velocity; colored surface: $u_\tau < 0$.

.

width of the tube around hyperplane and the "slack", respectively, see Section 1). Please recall that `svrLINEAR` is a linear method which gives a linear hyperplane. As can be seen in Fig.5, the predictions are not sensitive to C and ϵ. The RMS error, e, between the predicted friction velocity and the DNS database

$$e = \frac{\texttt{std}\left(u_{\tau,pred} - u_{\tau,DNS}\right)}{\texttt{mean}\left(u^2_{\tau,pred}\right)^{1/2}\texttt{mean}\left(u^2_{\tau,DNS}\right)^{1/2}} \tag{8}$$

is slightly below 20% for all `svr` and `svrLINEAR` cases (also for the standard wall functions). This error is rather high and it is discussed in Section 7. For `svrLINEAR`, I choose to use $C = 1$ and $\epsilon = 0.001$.

Figure 6 presents the friction velocities and the hyperplanes for two sets of C and ϵ, namely $\epsilon = 0.1$ and $C = 0.1$ (Fig. 7a) and $\epsilon = 0.1$ and $C = 0.01$ (Fig. 7b). First, we note that the hyperplanes are no longer linear since `svr` is a non-linear method. Second, the predicted friction velocities are strongly negative for $C = 0.1$ which is clearly unphysical (the smallest instantaneous friction velocity in the DNS database is $u_{\tau,min} = 0.11$). Decreasing C by a factor of 10 gives a much more reasonable hyperplane. As mentioned above, the RMS error (Eq. 8) is slightly below 20% also for this case which at first is somewhat surprising. However, when looking at the data in a 2D view we get the explanation: the area spanned by (Re and $(\partial\bar{U}/\partial y)_{non}$) in which the hyperplane for u_τ goes negative does not include any DNS values, see Fig. 7a. Figure 7b does not show any negative values of the hyperplane which we already observed in Fig. 7b. I choose to use $C = 0.1$ and $\epsilon = 0.01$.

It may be noted that Fig. 7 indicates a strong correlation between Re and $\left(\frac{\partial\bar{U}}{\partial y}\right)_{non}$. This is indeed the case. It turns out that the correlation coefficient (Eq. 10) is -0.45; this is further discussed in Section 7.

5.1 Python code

Here I present some of the Python commands. First, I scale the input data

```
scaler_dudy=StandardScaler()
scaler_re=StandardScaler()
scaler_yplus=StandardScaler()
dudy_in=scaler_dudy.fit_transform(dudy_in)
re_in=scaler_re.fit_transform(re_in)
yplus_in=scaler_yplus.fit_transform(yplus_in)
```

Then I put the input and output data on generic form

```
y=ustar_out                 # output
X=np.zeros((n_svr,3))
X[:,0]=re_in[:,0]           # 1st indata
X[:,1]=dudy_in[:,0]         # 2nd indata
X[:,2]=yplus_in[:,0]        # 3rd indata
```

Then I choose the model

```
C=1
eps=0.001
model = LinearSVR(max_iter=10000,epsilon = eps, C = C)
```

I train the model

```
svr = model.fit(X, y.flatten())
```

Now comes the testing part. I scale my test data

```
# Use MinMax scaling
dudy_in_test=dudy_in_test.reshape(-1, 1)
re_in_test=re_in_test.reshape(-1, 1)
yplus_in_test=yplus_in_test.reshape(-1, 1)
dudy_in_test=scaler_dudy.transform(dudy_in_test)
re_in_test=scaler_re.transform(re_in_test)
yplus_in_test=scaler_yplus.transform(yplus_in_test)
```

Then I predict friction velocities

```
y_svr = model.predict(X_test)
```

Now I want to find how accurate my predictions are. I compare with DNS data

```
# find difference
scale==np.mean(y_svr)*np.mean(ustar_out_test)
ustar_rms=np.std(y_svr-ustar_out_test)/scale
print('ustar_rms',ustar_rms)
```

Finally I store the model on disk.

```
# save the model to disk
dump(model, 'model-svrLINEAR.bin')
dump(scaler_re,'model-svrLINEAR_scaler-u.bin')
dump(scaler_dudy,'model-svrLINEAR_scaler-dudy.bin')
dump(scaler_yplus,'model-svrLINEAR_scaler-yplus.bin')
np.savetxt('min-max-model-svrLINEAR.txt', \
[dudy_min,dudy_max,re_max,re_min,yplus_max,yplus_min])
```

When I do the LES simulations with **pyCALC-LES** I load the model. Then when I predict the friction velocities, I do as in the testing phase above, except that

```
dudy_in_test
re_in_test
yplus_in_test
```

	LES with `svr`	LES with `svrLINEAR`
one time step	1.64	0.045
`svr` or `svrLINEAR` prediction	1.6	$1.2 \cdot 10^{-4}$

Table 3: Elapsed time in seconds.

at both walls are given by **pyCALC-LES** .

As you see above, I store `min` and `max` of all indata parameters. As a precaution, I limit the indata given by **pyCALC-LES** so that they stay within the limits of the DNS database, e.g.

```
dudy=np.minimum(dudy,dudy_max)
dudy=np.maximum(dudy,dudy_min)
```

6 Results

Here I evaluate `svr` and `svrLINEAR` in fully-developed channel flow at two different Reynolds numbers, namely $Re_\tau = 2\,000$ and $Re_\tau = 5\,200$. For the lower Reynolds number I use a proper wall functions grid (i.e. wall-adjacent cells at $\langle y^+ \rangle = 55$) whereas I for the higher Reynolds also use grids i.e. which are not really suitable for wall functions (wall-adjacent cells at $\langle y^+ \rangle = 15$ and $\langle y^+ \rangle = 8$).

The extent of the domain in the x and z direction is 3.2 and 1.6, respectively, covered by 32 cells in each direction. The Python code **pyCALC-LES** is used for all simulations together with the Smagorinsky model, see Section 3.

6.1 $Re_\tau = 2\,000$

36 cells ($N_y = 36$, constant grid spacing) are used in the wall-normal direction which gives $\langle y^+ \rangle = 55$ for the wall-adjacent cells. The DNS database defined in Table 1 is used. Figure 8 presents the predicted velocities. The `svrLINEAR` – using one, two or three influence parameters (see p. 9), `svr` and the standard wall functions are compared with Reichardt's law

$$U^+ = \frac{1}{\kappa} \ln(1-0.4y^+) + 7.8 \left[1 - \exp\left(-y^+/11\right) - (y^+/11) \exp\left(-y^+/3\right)\right] \quad (9)$$

The agreement is excellent for all cases except for `svrLINEAR` when only one influence parameter (Re) is used. The resolved stresses are compared with DNS in Fig. 9 and the agreement is reasonable.

The conclusion for this test case is that both `svr` and `svrLINEAR` (and the standard wall functions) give excellent agreement with benchmark data. However, the required CPU time for `svr` and `svrLINEAR` differ greatly. Table 3 presents the elapsed time. As can be seen, the required time for the `svr` is five orders of

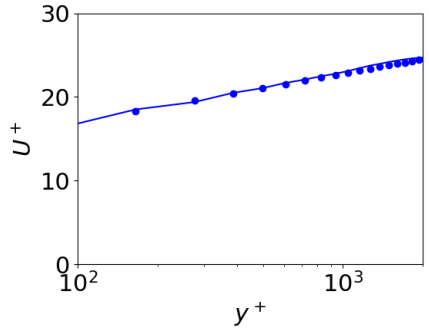

(a) Standard wall functions.

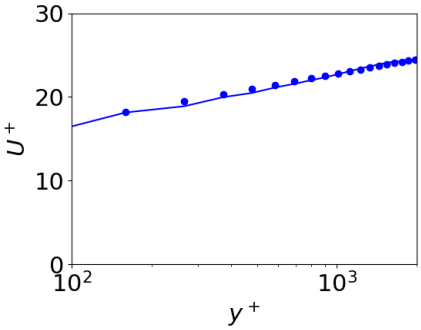

(b) `svrLINEAR`. With $\langle y^+ \rangle$, with $\left(\frac{\partial \bar{U}}{\partial y}\right)_{non}$

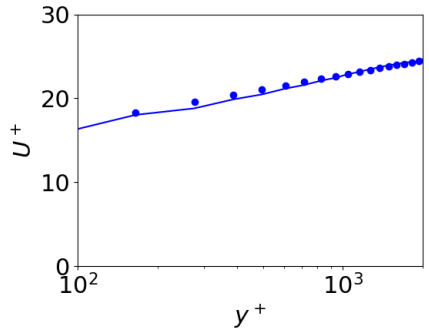

(c) `svrLINEAR`. With $\langle y^+ \rangle$, no $\left(\frac{\partial \bar{U}}{\partial y}\right)_{non}$

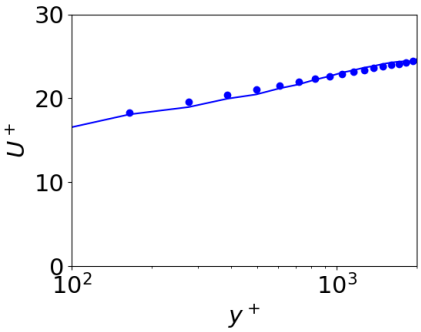

(d) `svrLINEAR`. No $\langle y^+ \rangle$, with $\left(\frac{\partial \bar{U}}{\partial y}\right)_{non}$

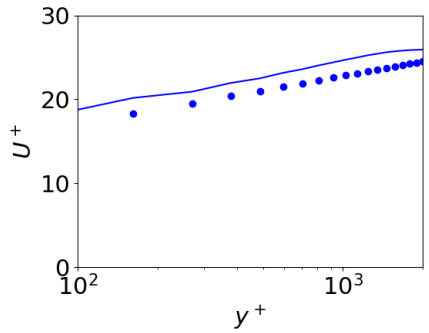

(e) `svrLINEAR`. No $\langle y^+ \rangle$, no $\left(\frac{\partial \bar{U}}{\partial y}\right)_{non}$

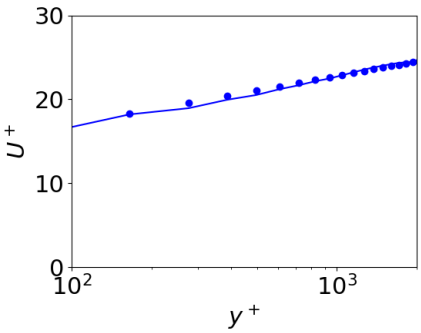

(f) `svr`. No $\langle y^+ \rangle$, with $\left(\frac{\partial \bar{U}}{\partial y}\right)_{non}$

Figure 8: Channel flow. $Re_\tau = 2\,000$. Velocity. $N_y = 36$. Re is used as influence parameters for all `svr` and `svrLINEAR` cases. •: Reichardt's law, Eq. 9.

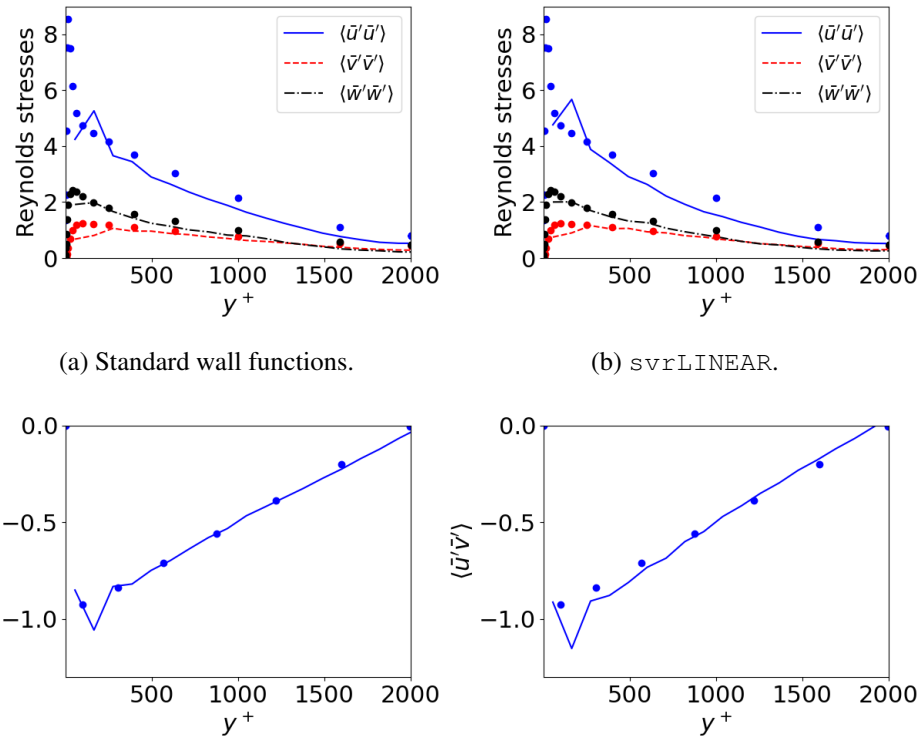

(a) Standard wall functions.

(b) `svrLINEAR`.

(c) Standard wall functions.

(d) `svrLINEAR`.

Figure 9: Channel flow. $Re_\tau = 2\,000$. $N_y = 36$. Reynolds stresses. Re, $\langle y^+ \rangle$ and $\left(\frac{\partial \bar{U}}{\partial y}\right)_{non}$ are used as influence parameters for `svrLINEAR`.

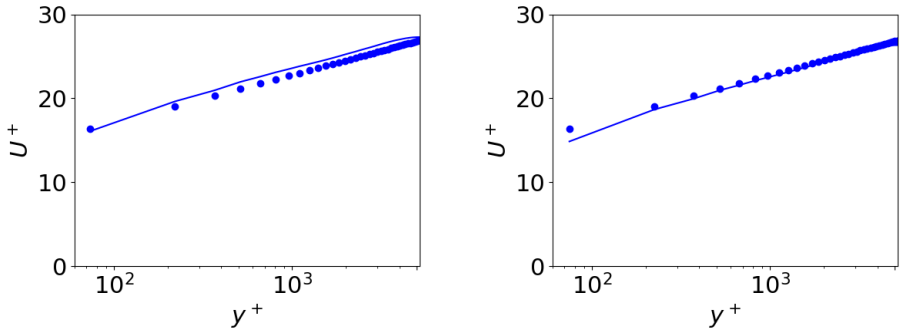

(a) Standard wall functions. (b) `svrLINEAR`.

Figure 10: Channel flow. $Re_\tau = 5,200$. Velocity. $N_y = 70$. All three influence parameters are used for `svrLINEAR`. •: Reichardt's law, Eq. 9

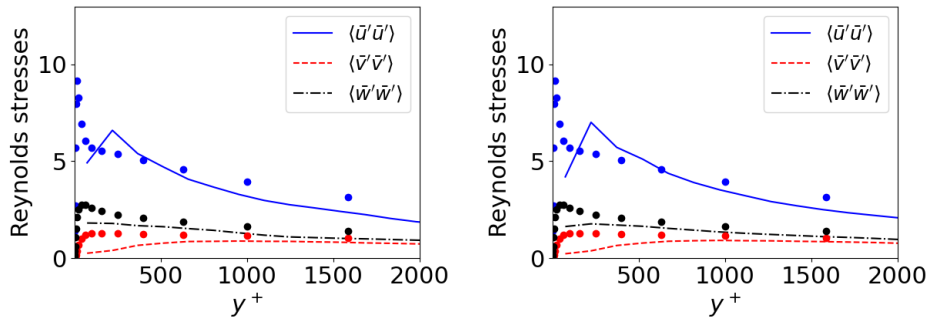

(a) Standard wall functions. (b) `svrLINEAR`.

Figure 11: Channel flow. $Re_\tau = 5\,200$. $N_y = 70$. Reynolds stresses. All three influence parameters are used for `svrLINEAR`.

magnitude larger than `svrLINEAR`. As I mentioned in Section 5, I use 10 000 samples in each of the six locations (i.e. 10 1000). This number could most likely be reduced. But let's wait until we have looked at the results of the other channel flow simulations below.

6.2 $Re_\tau = 5\,200$

70 cells ($N_y = 70$, constant grid spacing) are used in the wall-normal direction which gives $\langle y^+ \rangle = 74$ for the wall-adjacent cells. The DNS database defined in Table 1 is used. Figure 10 presents the predicted velocity profile and the agreement with Reichardt's lawis very good (slightly better for `svr` than the standard wall function). The Reynolds stresses are shown in Fig. 11 and both method give fairly good agreement with DNS.

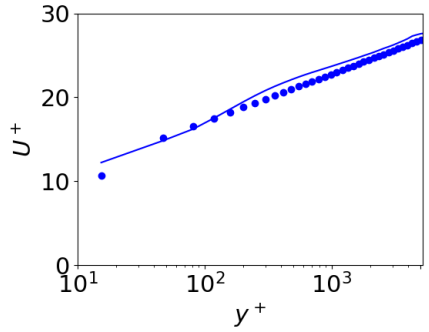

(a) Standard wall functions.

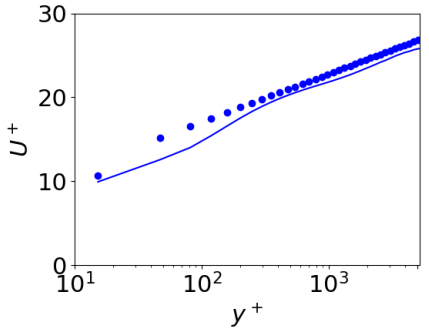

(b) `svrLINEAR` with $\langle y^+ \rangle$, with $\left(\frac{\partial \bar{U}}{\partial y}\right)_{non}$.

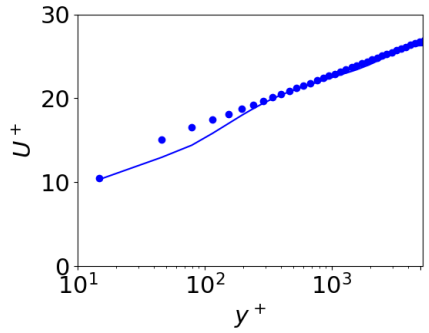

(c) `svrLINEAR` with $\langle y^+ \rangle$, no $\left(\frac{\partial \bar{U}}{\partial y}\right)_{non}$.

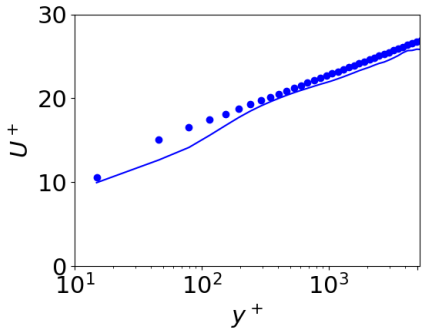

(d) `svr` with $\langle y^+ \rangle$, no $\left(\frac{\partial \bar{U}}{\partial y}\right)_{non}$.

Figure 12: Channel flow. $Re_\tau = 5\,200$. $N_y = 70$. Velocity. Stretching in y direction: 1.08. Re is used as influence parameters for all `svr` and `svrLINEAR` cases. •: Reichardt's law, Eq. 9.

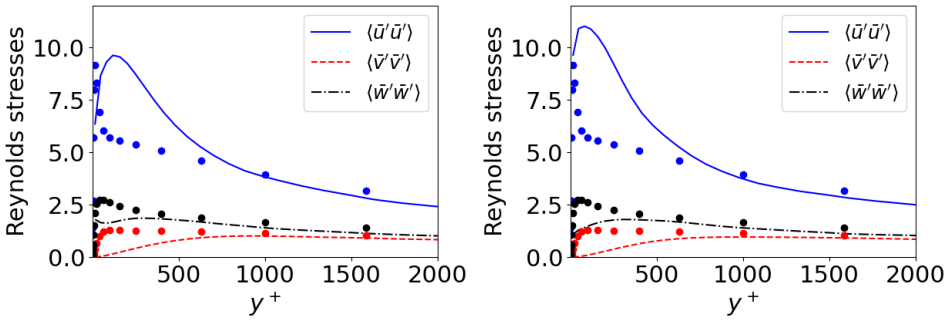

(a) Standard wall functions.

(b) `svrLINEAR`.

Figure 13: Channel flow. $Re_\tau = 5\,200$. $N_y = 70$. Stretching in y direction: 1.08. Reynolds stresses. Re, $\langle y^+\rangle$ and $\left(\frac{\partial \bar{U}}{\partial y}\right)_{non}$ are used as influence parameters for `svrLINEAR`. •: DNS data (Lee and Moser, 2015)

6.3 $Re_\tau = 5\,200$ with a stretching of 1.08.

Here I will present LES simulation at $Re_\tau = 5\,200$ with $N_y = 70$ and a stretching of the grid in the wall-normal direction of 1.08. This gives $\langle y^+\rangle = 15$ at the wall-adjacent cells. The DNS database defined in Table 2 is used.

Figure 12 show predicted velocities with the standard wall functions, `svr` and `svrLINEAR`. `svrLINEAR` including $\left(\frac{\partial \bar{U}}{\partial y}\right)_{non}$ (Fig. 12b) gives poorest agreement with Reichardt's law. `svrLINEAR` with Re and $\langle y^+\rangle$ shows best performance (Fig. 12c), slightly better than the standard wall functions. Figure 13 compares the normal stresses with the DNS stresses. The stresses obtained with both methods gives too large streamwise stresses and too small wall-normal and spanwise stresses.

6.4 $Re_\tau = 5\,200$ with a stretching of 1.11.

Here I present the last LES simulations; the Reynolds number is $Re_\tau = 5\,200$ with $N_y = 70$ and a stretching of the grid in the wall-normal direction of 1.11. This moves the wall-adjacent cells even closer to the wall so that $\langle y^+ = 8\rangle$. The DNS database defined in Table 2 is used. The predicted velocities are shown in Fig. 14; The best agreement is shown by `svrLINEAR` with Re and $\langle y^+\rangle$ as influence parameters (Fig. 14c); standard wall functions give almost as good agreement (Fig. 14a). The non-linear `svr` gives poor agreement. The Reynolds stresses (Fig. 15) predicted show the same pattern as in Fig. 13: too large streamwise stresses (slightly larger for `svrLINEAR`) and $\langle\bar{v}'\bar{v}'\rangle$ and $\langle\bar{w}'\bar{w}'\rangle$ too small.

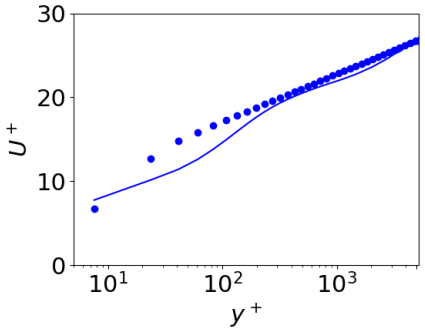

(a) Standard wall functions.

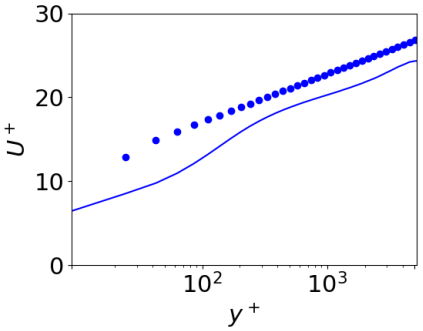

(b) `svrLINEAR` with $\langle y^+ \rangle$, with $\left(\frac{\partial \bar{U}}{\partial y}\right)_{non}$.

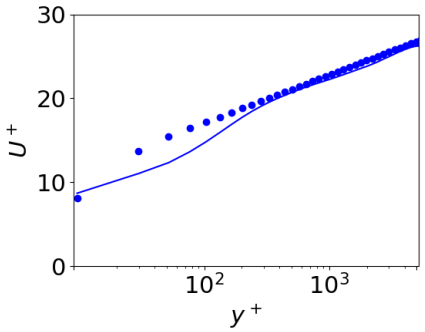

(c) `svrLINEAR` with $\langle y^+ \rangle$, no $\left(\frac{\partial \bar{U}}{\partial y}\right)_{non}$.

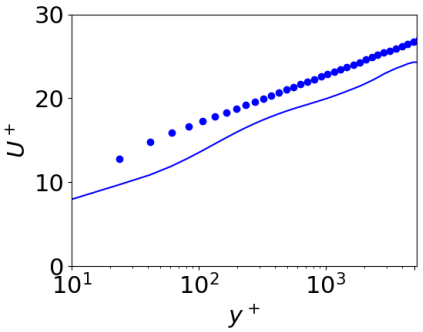

(d) `svr`. With $\langle y^+ \rangle$, no $\left(\frac{\partial \bar{U}}{\partial y}\right)_{non}$.

Figure 14: Channel flow. $Re_\tau = 5\,200$. $N_y = 70$. Velocity. Stretching in y direction: 1.11. Re is used as influence parameters for all `svr` and `svrLINEAR` cases. •: Reichardt's law, Eq. 9.

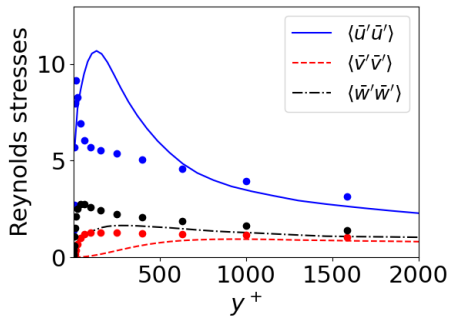

(a) Standard wall functions.

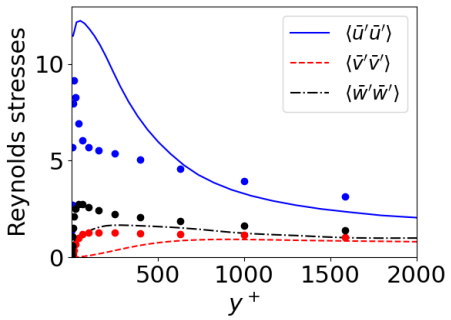

(b) `svrLINEAR` with $\langle y^+ \rangle$, no $\left(\frac{\partial \bar{U}}{\partial y}\right)_{non}$.

Figure 15: Channel flow. $Re_\tau = 5\,200$. $N_y = 70$. Stretching in y direction: 1.11. Reynolds stresses. •: DNS data (Lee and Moser, 2015)

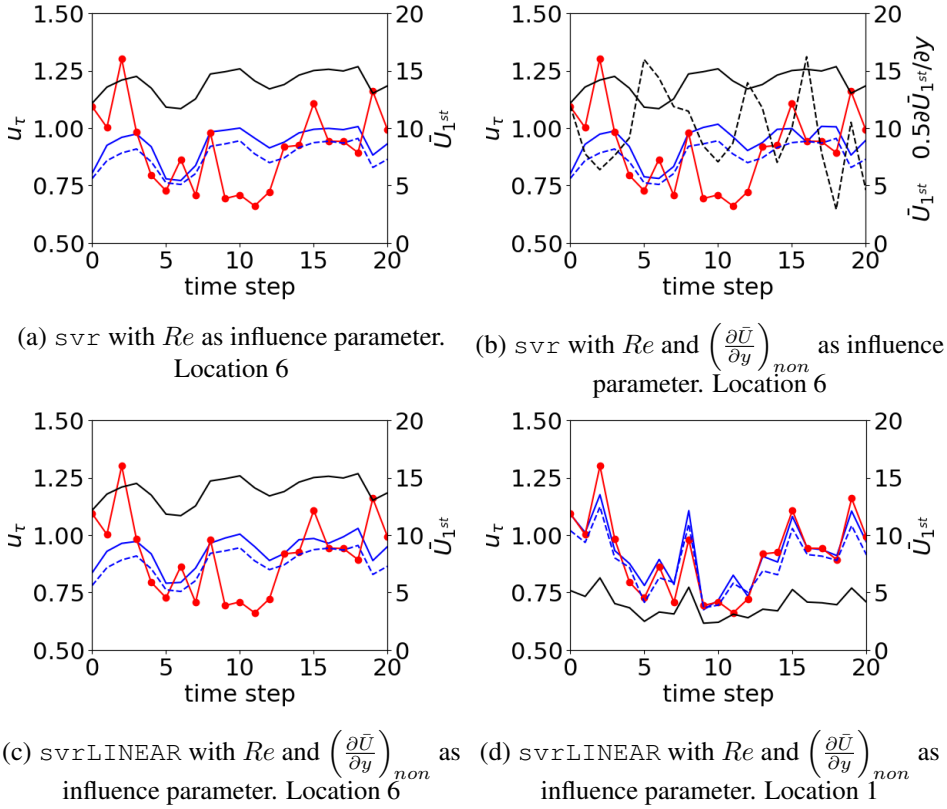

(a) `svr` with Re as influence parameter. Location 6

(b) `svr` with Re and $\left(\frac{\partial\bar{U}}{\partial y}\right)_{non}$ as influence parameter. Location 6

(c) `svrLINEAR` with Re and $\left(\frac{\partial\bar{U}}{\partial y}\right)_{non}$ as influence parameter. Location 6

(d) `svrLINEAR` with Re and $\left(\frac{\partial\bar{U}}{\partial y}\right)_{non}$ as influence parameter. Location 1

Figure 16: Testing of `svrLINEAR` and `svr` at Location 1 and 6, see Table 1. ——: u_τ from `svrLINEAR` or `svr`; - - -: u_τ from the standard wall functions; •: DNS database; ——: $\bar{U}_{1^{st}}$; ▬ ▬: $\partial\bar{U}_{1^{st}}/\partial y$.

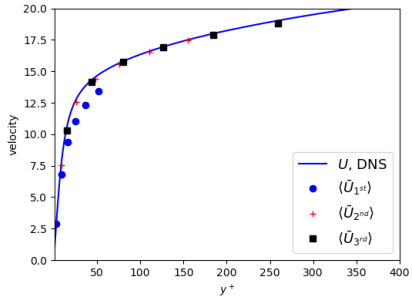

Figure 17: Averaged streamwise velocity from the DNS database and predicted by `svr`.

7 Conclusions

Machine learning methods have been used to develop new wall functions. Support Vector Regression methods are employed, both non-linear, `svr`, and linear, `svrLINEAR`, which are available in Python. A DNS database created from fully-developed channel flow has been used for training and testing the `svr` and the `svrLINEAR`. When the wall-adjacent cells are located in the log-law region, both `svr` and `svrLINEAR` give perfect agreement with the Reichardt's law (as does the standard wall functions). When the wall-adjacent cells are located in the buffer layer, `svrLINEAR` gives better agreement with the Reichardt's law than the standard wall functions, but the agreement is not perfect. It is found that `svrLINEAR` gives better agreement with the Reichardt's law than `svr`, in some cases much better. Furthermore, `svr` requires computer times that is orders of magnitude larger than `svrLINEAR`; it is found that the `svr` may dominate the CPU/GPU time for one time step, see Table 3. This problem could probably be reduced by using a smaller training set, but since `svrLINEAR` anyway is more accurate than `svr`, no such attempt has been made.

I find in Section 5 that the error (Eq. 8) of all `svr` and `svrLINEAR` methods – and the standard wall functions – is close to 20%. That is rather high. The predicted friction velocity for 20 time steps using `svrLINEAR` and `svr` are compared with the DNS database at Location 6, see Table 1. I also show u_τ obtained from the standard wall functions. Start by looking at Fig. 16a. We find that u_τ obtained from the wall functions closely follows the variation of $\bar{U}_{1^{st}}$. This applies also for the `svr` predicted friction velocity which is not surprising since Re (which is linearly related to $\bar{U}_{1^{st}}$) is used as influence parameter. Next, we turn to Fig. 16b where the influence parameter $\left(\frac{\partial \bar{U}}{\partial y}\right)_{non}$ is also used. It is somewhat surprising that the prediction by `svr` is virtually identical to that in Fig. 16a (there is a small difference at time step 16). Closer inspection of Fig. 16b reveals that there is a negative correlation between $\bar{U}_{1^{st}}$ and $\partial \bar{U}_{1^{st}}/\partial y$. Computing the correlation coefficient, e_c,

$$e_c\left(\bar{U}'_{1^{st}}, \partial \bar{U}'_{1^{st}}/\partial y\right) = \frac{\texttt{dot}\left(\bar{U}'_{1^{st}},\ \partial \bar{U}'_{1^{st}}/\partial y\right)}{\texttt{mean}\left(\bar{U}'^2_{1^{st}}\right)^{1/2}\texttt{mean}\left(\left(\partial \bar{U}'_{1^{st}}/\partial y\right)^2\right)^{1/2}} \tag{10}$$

(`dot` is Python's element-wise multiplication command) gives $e_c = -0.45$. The corresponding correlation coefficient between $\bar{U}_{1^{st}}$ and the u_τ predicted by `svr` is 0.41. Hence, it can be concluded that since $\bar{U}_{1^{st}}$ and $\partial \bar{U}_{1^{st}}/\partial y$ are fairly strongly correlated it does not make sense to use both as influence parameters. Now, let's look at the third figure (Fig. 16c) we find that the friction velocity by `svrLINEAR` is very similar to `svr` (Fig. 16b). A general observation in Fig. 16 is that the agreement between DNS data and `svr` (and `svrLINEAR`) in Fig. 16 is poor. Why? We can see that the time scales of the friction velocity from the DNS database is much smaller than in those by `svr` and `svrLINEAR`. The reason is that the friction velocity in the DNS database'is computed over only one DNS cell for which

$\Delta x^+_{DNS} = 13$ and $\Delta z^+_{DNS} = 6.5$ which should be compared with $2\Delta y = 170$ at Location 6 (see Fig. 3 and Table 1). However, the predicted friction velocity with `svrLINEAR` at Location 1 (Fig. 16d) for which $2\Delta y = 10$ (which is close to Δx^+_{DNS} and Δz^+_{DNS}) agrees well with the DNS database. This is a strong indication that the friction velocity in the DNS database should be integrated over $\Delta x \simeq 2\Delta y$ and $\Delta z \simeq 2\Delta y$. This means that the friction velocity in the DNS database will be different for the six different locations, see Tables 1 and 2.

The averaged filtered velocities (see Eqs. 3 and 7) are shown in Fig. 17. It is seen that $\bar{U}_{1^{st}}$ does not agree with the DNS velocity profile whereas the agreement for $\bar{U}_{2^{nd}}$ and $\bar{U}_{3^{rd}}$ is perfect. The reason is that the gradient of the DNS data near the wall is very large and since $\bar{U}_{1^{st}}$ is computed by integrating from the wall to $2\Delta y$ the integrated value differs much from the local (i.e. DNS) value. Maybe it is best to avoid using the first cell, $\bar{U}_{1^{st}}$, and instead rely on $\bar{U}_{2^{nd}}$ and $\bar{U}_{3^{rd}}$ as proposed by Kawai1 and Larsson (2012); Mukha et al. (2021).

I have here presented – as indicated in the title – my first attempt. In my next attempt I will create the DNS database by integrating the friction velocities over suitable Δx and Δz (I've already started). It would also be interesting to develop machine-learning wall functions for heat transfer. To extend the method to recirculating flow is the next – but very challenging – step.

Acknowledgments

This study was partly financed by *Strategic research project on Chalmers on hydro- and aerodynamics*.

The computations were enabled by resources provided by the Swedish National Infrastructure for Computing (SNIC) at NSC partially funded by the Swedish Research Council through grant agreement no. 2018-05973.

References

L. Davidson. CALC-LES: a Fortran code for LES and hybrid LES-RANS. Technical report, Division of Fluid Dynamics, Dept. of Mechanics and Maritime Sciences, Chalmers University of Technology, Gothenburg, 2018.

L. Davidson. pyCALC-LES: a Python code for DNS, LES and Hybrid LES-RANS. Division of Fluid Dynamics, Dept. of Mechanics and Maritime Sciences, Chalmers University of Technology, Gothenburg, 2021.

Lars Davidson and Shia-Hui Peng. Hybrid LES-RANS: A one-equation SGS model combined with a $k-\omega$ for predicting recirculating flows. *International Journal for Numerical Methods in Fluids*, 43(9):1003–1018, 2003.

J. Dominique, J. Van den Berghe, C. Schram, and M. A. Mendez. Artificial neural networks modeling of wall pressure spectra beneath turbulent boundary layers.

Physics of Fluids, 34(3):035119, 2022. doi: 10.1063/5.0083241. URL https://doi.org/10.1063/5.0083241.

P. Emvin. *The Full Multigrid Method Applied to Turbulent Flow in Ventilated Enclosures Using Structured and Unstructured Grids*. PhD thesis, Dept. of Thermo and Fluid Dynamics, Chalmers University of Technology, Göteborg, 1997.

Soshi Kawai1 and Johan Larsson. Wall-modeling in large eddy simulation: Length scales, grid resolution, and accuracy. *Physics of Fluids*, 24:015105, 2012. URL https://doi.org/10.1063/1.3678331.

M. Lee and R. D. Moser. Direct numerical simulation of turbulent channel flow up to $Re_\tau \approx 5200$. *Journal of Fluid Mechanics*, 774:395–415, 2015. doi: 10.1017/jfm.2015.268. URL https://doi.org/10.1017/jfm.2015.268.

Andreas Lindholm, Niklas Wahlström, Fredrik Lindsten, and Thomas Schön. *Machine Learning: A First Course for Engineers and Scientists*. Cambridge University Press, 03 2022. ISBN 9781108843607. doi: 10.1017/9781108919371. URL https://doi.org/10.1017/9781108919371.

Julia Ling, Matthew F. Barone, Warren Davis, Kamaljit Chowdhary, and Jeffrey Fike. Development of machine learning models for turbulent wall pressure fluctuations. In *55th AIAA Aerospace Sciences Meeting*, 2017. doi: 10.2514/6.2017-s̄0755. URL https://arc.aiaa.org/doi/abs/10.2514/6.2017-s̄0755.

T. Mukha, R.E. Bensow, and M. Liefvendahl. Predictive accuracy of wall-modelled large-eddy simulation on unstructured grids. *Computers & Fluids*, 221:104885, 2021. ISSN 0045-7930. doi: https://doi.org/10.1016/j.compfluid.2021.104885. URL https://www.sciencedirect.com/science/article/pii/S0045793021000517.

L. N. Olson and J. B. Schroder. PyAMG: Algebraic multigrid solvers in Python v4.0, 2018. URL https://github.com/pyamg/pyamg. Release 4.0.

Menneni Rachana, Jegadeesan Ramalingam, Gajula Ramana, Adigoppula Tejaswi, Sagar Mamidala, and G Srikanth. Fraud detection of credit card using machine learning. *GIS-Zeitschrift für Geoinformatik*, 8:1421–1436, 10 2021.

Sudarshana S Rao and Santosh R Desai. Machine learning based traffic light detection and ir sensor based proximity sensing for autonomous cars. In *Proceedings of the International Conference on IoT Based Control Networks & Intelligent Systems – ICICNIS*, 2021. URL http://dx.doi.org/10.2139/ssrn.3883931.

M. Tanahashi, S.-J. Kang, T. Miyamoto, S. Shiokawa, and T. Miyauchi. Scaling law of fine scale eddies in turbulent channel flows up to $re_\tau =$

800. *International Journal of Heat and Fluid Flow*, 25(3):331–340, 2004. ISSN 0142-727X. doi: https://doi.org/10.1016/j.ijheatfluidflow.2004.02.016. URL https://www.sciencedirect.com/science/article/pii/S0142727X04000074. Turbulence and Shear Flow Phenomena (TSFP-3).

Lorenzo Tieghi, Alessandro Corsini, Giovanni Delibra, and Francesco Aldo Tucci. A machine-learnt wall function for rotating diffusers. volume Volume 1: Aircraft Engine; Fans and Blowers of *Turbo Expo: Power for Land, Sea, and Air*, 09 2020. doi: 10.1115/GT2020-s̄15353. URL https://doi.org/10.1115/GT2020-s̄15353.